Satellite SAR wind resource mapping in China (SAR-China)

Badger, Merete

Publication date:
2009

Document Version
Publisher's PDF, also known as Version of record

Satellite SAR wind resource mapping in China

(SAR-China)

Risø-R-Report

Merete Badger
Risø-R-1706(EN)
July 2009

Risø DTU
National Laboratory for Sustainable Energy

Author: Merete Badger
Title: Satellite SAR wind resource mapping in China (SAR-China)
Division: Wind Energy Division

Risø-R-1706(EN)
July 2009

Abstract (max. 2000 char.):

The project 'Off-Shore Wind Energy Resource Assessment and Feasibility Study of Off-Shore Wind Farm Development in China' is funded by the EU-China Energy and Environment Programme (EEP) and runs for one year (August 2008 - August 2009). The project is lead by the China Meteorological Administration (CMA) and supported by SgurrEnergy Ltd. Risø National Laboratory for Sustainable Energy at the Technical University of Denmark (Risø DTU) has been commissioned to perform a satellite based wind resource analysis as part of the project. The objective of this analysis is to map the wind resource offshore at a high spatial resolution (1 km). The detailed wind resource maps will be used, in combination with other data sets, for an assessment of potential sites for offshore wind farm development along the coastline from Fujian to Shandong in China.

ISSN 0106-2840
ISBN 978-87-550-3772-4

Contract no.:

Group's own reg. no.:
1130610-06

Sponsorship: EU-China Energy and Environment Programme (EEP). Data provided by the European Space Agency.

Cover :

Pages: 17
Tables: 1
References: 11

Information Service Department
Risø National Laboratory for Sustainable Energy
Technical University of Denmark
P.O.Box 49
DK-4000 Roskilde
Denmark
Telephone +45 46774005
bibl@risoe.dtu.dk
Fax +45 46774013
www.risoe.dtu.dk

Contents

Preface 4

1 Introduction 5

2 Satellite data 6

3 SAR wind retrieval 7

4 Statistical analysis 9

4.1 Field statistics 10
4.2 Site statistics 14

5 Conclusion 15

Preface

The project 'Off-Shore Wind Energy Resource Assessment and Feasibility Study of Off-Shore Wind Farm Development in China' is funded by the EU-China Energy and Environment Programme (EEP) and runs for one year (August 2008 - August 2009). The project is lead by the China Meteorological Administration (CMA) and supported by SgurrEnergy Ltd. Risø National Laboratory for Sustainable Energy at the Technical University of Denmark (Risø DTU) has been commissioned to perform a satellite based wind resource analysis as part of the project. The objective of this analysis is to map the wind resource offshore at a high spatial resolution (1 km). The detailed wind resource maps will be used, in combination with other data sets, for an assessment of potential sites for offshore wind farm development along the coastline from Fujian to Shandong in China.

1 Introduction

The project 'Off-Shore Wind Energy Resource Assessment and Feasibility Study of Off-Shore Wind Farm Development in China' covers about 10.000 km of coastline from Fujian to Shandong in China. The satellite based wind resource mapping carried out by Risø DTU was restricted to a smaller section of coastline covering Jiangsu and Shanghai. The map in Figure 1 shows the section selected for satellite based wind mapping.

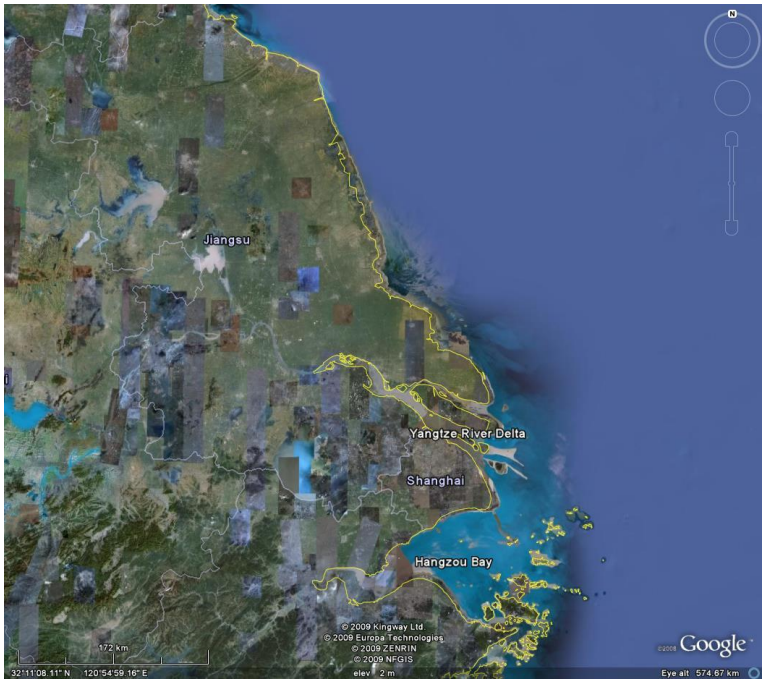

Figure 1. Map showing the coastline of Jiangsu and Shanghai provinces in China. A satellite based wind resource analysis was made for this stretch of coastline, which is approximately 600 km measured in a straight line. Image courtesy Google Earth.

The analysis was based on satellite synthetic aperture radar (SAR) data from the European Space Agency (ESA). The major advantage of using satellite SAR data for offshore wind mapping lies in the high spatial resolution of the data and the coverage of coastal waters. Wind fields can be retrieved from SAR at a resolution of <1 km. Other wind products from satellite (i.e. scatterometer or passive microwave data) have a coarser resolution and no coverage within the first ~25 km from the coastline. Unlike global-coverage satellite observations SAR data are not acquired on a regular basis over a given point of interest. A major challenge associated with wind resource mapping from SAR is to obtain a sufficient number of SAR samples for a robust statistical analysis (Hasager et al., 2008).

The area selected for the satellite based wind resource analysis includes the Hangzhou Bay to the south and Yangtze River Delta to the north of Shanghai. Wind mapping from SAR is generally more accurate over the open ocean than over enclosed seas. A lower accuracy of the SAR wind retrievals was thus anticipated for the Hangzhou Bay and the Yangtze River Delta.

To the east of Jiangsu (around 121E, 32.5N) is a large area with shallow waters and mobile sand banks. The sand banks are partly exposed and represent a major constraint for successful satellite based wind mapping. The problems related to enclosed seas and exposed sand bars were pointed out by Risø DTU in the initial phase of the project. A decision was made to include the problematic areas in the satellite based wind resource analysis, as these areas cover several potential wind farm sites.

2 Satellite data

The wind resource mapping was based on satellite SAR data from the ESA's ENVISAT mission (2002-present, see also http://www.envisat.esa.int/). A total of 200 archived SAR images were granted for the project through an ESA Category-1 research proposal. Additional images were obtained from the ENVISAT systematic mission, which is a rolling archive containing data from the last 15 days. All images were acquired in ENVISAT's Wide Swath Mode (WSM) covering an area of 400 km by 400 km with a ~150 m pixel spacing.

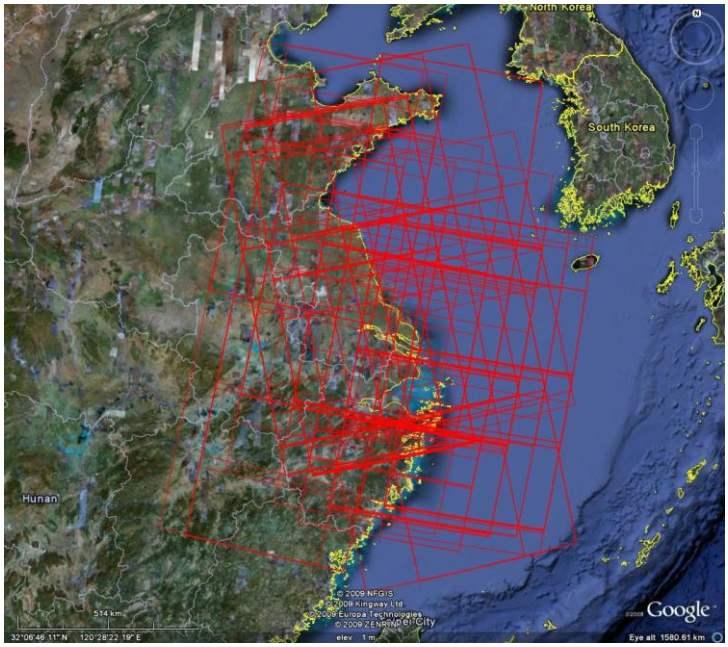

Figure 2. Satellite footprints for the 147 selected ENVISAT ASAR WSM scenes. Each satellite scene covers 400 km by 400 km with a ~150 km pixel spacing. Image courtesy Google Earth.

The archived satellite data were selected and ordered by CMA from ESA's on-line catalogue EOLI-SA. An initial check showed that approximately 300 satellite scenes were available in the desired format over the area of interest. During the image selection procedure it became clear that only 147 of the available images were suitable for the wind resource analysis, based on their spatial coverage. The rest of the archived images covered only a small part of the area of interest, or they had a large fraction of land pixels. The coverage of the 147 selected images is seen in Figure 2.

3 SAR wind retrieval

An example of a raw satellite SAR image showing image intensities over the area of interest in China is seen in Figure 3. Over the ocean, the image intensity increases with higher wind speeds because the radar signal interacts with cm-scale waves at the sea surface. These waves are generated by the local wind (Monaldo & Beal, 2004). The image intensity also depends on the radar incidence angle. A systematic increase of the intensity is therefore seen from left (far-range) to right (near-range) across the image in Figure 3. This effect is taken into account in the processing of SAR images to wind fields. In the following we summarize the processing of SAR data to maps of wind speed. A more detailed description of wind retrievals from SAR is given in Christiansen et al. (2008) and references therein.

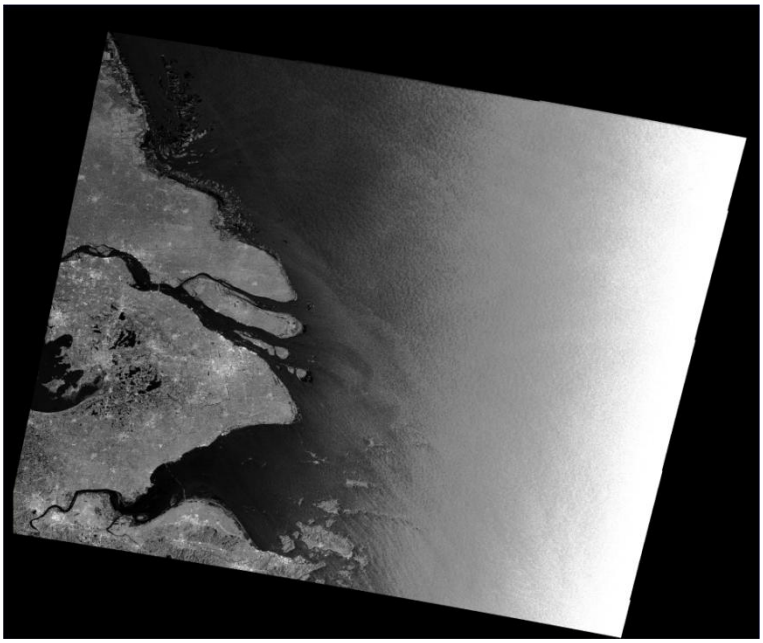

Figure 3. ENVISAT ASAR intensity image acquired over the area of interest in China on January 31, 2005.

Each satellite image was calibrated to show radar backscatter coefficients. Pixels were averaged to a size of ~1 km in order to reduce effects of longer-period oceanic waves and random image noise (i.e. speckle). Wind fields were then retrieved from the radar backscatter images by inversion of an empirical geophysical model function (GMF):

$$\sigma^0 = U^{\gamma(\theta)} A(\theta) \left[1 + B(\theta, U)\cos\phi + C(\theta, U)\cos 2\phi\right] \qquad (1)$$

where σ^0 is the radar backscatter coefficient, U is wind speed at the height 10 m for a neutrally-stratified atmosphere, θ is the local incidence angle, and ϕ is the wind direction with respect to the radar look direction. A, B, C, and γ are empirical coefficients that vary for different GMFs. The most recent model function, CMOD5, was used for the wind retrievals in this project (Hersbach et al., 2007). A study at a Danish offshore site has shown that winds can be retrieved from CMOD5 with an accuracy of ±1.34 m/s on the 10-m wind speed (Christiansen et al., 2006).

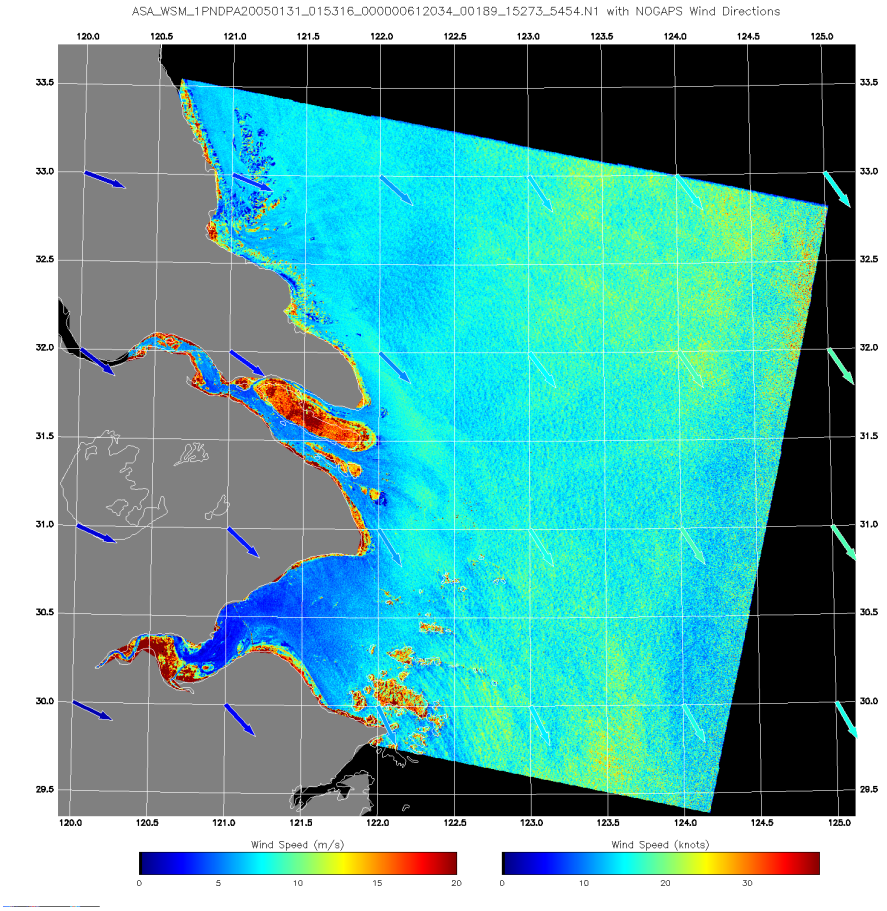

Figure 4. Wind field retrieved at 10 m from an ENVISAT satellite scene of January 31, 2005. Arrows show NOGAPS model wind fields using the same colour scale.

Several wind speed and direction pairs correspond to a given value of σ^0 in Equation 1. However, it is possible to solve the equation for wind speed if the wind direction is known. In this project, the wind inversion was initiated using 6-hourly wind directions from the US Navy Operational Global Atmospheric Prediction System (NOGAPS). The NOGAPS data have a spatial resolution of 1º latitude/longitude and were interpolated in time and space to match the satellite observations.

For 11 of the 147 satellite SAR scenes no matching NOGAPS data could be found and CMA provided model wind fields instead. For these satellite scenes, wind inversion was performed with a constant wind direction for the entire image. The wind directions were obtained from the model grid point located at 122.5E, 32 N and they are listed in Table 1.

Data file	Model wind direction
ASA_WSM_1PNDPA20030117_020701_000000612013_00046_04609_5377.N1	141
ASA_WSM_1PNDPA20030127_015311_000000612013_00189_04752_5379.N1	139
ASA_WSM_1PNDPA20031119_015022_000000612021_00418_08989_5391.N1	244
ASA_WSM_1PNDPA20031122_015523_000000612021_00461_09032_5663.N1	217
ASA_WSM_1PNDPA20031122_015623_000000612021_00461_09032_5677.N1	217
ASA_WSM_1PNDPA20050128_014733_000000612034_00146_15230_5452.N1	265
ASA_WSM_1PNDPA20060520_015601_000000612047_00461_22058_5555.N1	17
ASA_WSM_1PNUPA20040218_134157_000000612024_00225_10299_9278.N1	312
ASA_WSM_1PNUPA20040501_134741_000000612026_00268_11344_9242.N1	305
ASA_WSM_1PNUPA20040504_135318_000000612026_00311_11387_9288.N1	118
ASA_WSM_1PNUPA20040505_020940_000000612026_00318_11394_2785.N1	41
ASA_WSM_1PNUPA20070628_015852_000000612059_00232_27841_9912.N1	34

Table 1. List of SAR-scenes that were processed with a constant model wind direction provided by CMA. The wind directions are in degrees from north.

The SAR data were processed to wind maps using the APL/NOAA SAR Wind Retrieval Software (ANSWRS) developed at the Johns Hopkins University, Applied Physics Laboratory (JHU/APL) (Monaldo et al., 2005). Risø DTU holds a license to use this tool. Figure 4 shows a wind field retrieved from the satellite SAR image in Figure 3. Each wind map was delivered as an image file (.png) and a Google Earth file (.kmz).

4 Statistical analysis

The 147 satellite SAR wind maps were combined for a statistical analysis of the wind resource. The analysis was performed with the S-WAsP tool developed at Risø DTU. This tool fits a Weibull function to a number of wind observations for each grid cell within a specified domain (Nielsen et al., 2004; Hasager et al., 2005; Hasager et al., 2006). A robust statistical analysis relies on 100 or more overlapping satellite samples for each grid cell (Barthelmie & Pryor, 2003; Pryor et al., 2003).

The statistical analysis results in maps of the mean wind speed, energy density[1], and the Weibull scale and shape parameters (A and k). This collection of maps is called 'field statistics'. The maps and associated parameters are delivered as one multi-layer file in .cdf format. The map projection used by S-WAsP is UTM with datum WGS 84.

More detailed statistics can be obtained for selected sites of special interest e.g. an offshore mast position or a potential wind farm site. The site statistics are delivered as a report (.txt format) and as a .tab file. The latter can be analysed further in the Wind Atlas Analysis and Application Programme (WAsP, see also www.wasp.dk) in order to estimate wind farm energy production.

4.1 Field statistics

In this project, field statistics were computed at a spatial resolution of 1km for the domain covered by the map in Figure 5. The map shows the number of overlapping satellite images for each 1 km grid cell. The best covered cells within the domain had 101 samples. There are generally 70 or more samples along the coastline of Shanghai and the southern part of Jiangsu. Unfortunately, the coverage is poorer (< 50) along the coastline of northern Jiangsu. The statistical analysis of SAR imagery is not reliable for areas with poor coverage, as single events with high or low wind speeds become very dominant. In the following we focus on a smaller domain where there are always 70 or more satellite samples. This domain is shown in Figure 5 bounded by a white rectangle.

The field statistics within the smaller domain were post-processed for better visualization of the results. The post-processing was performed in four steps:

1. Conversion of map projection from UTM zone 51 to a uniform latitude-longitude grid. For both projections, the datum was WGS 84.

2. Conversion of the S-WAsP 'energy density' to unit W/m^2 using the equation $E = \frac{1}{2} \rho \overline{u^3}$, where ρ is the air density and $\overline{u^3}$ is the mean value of the third power of the wind speed. The value of ρ was assumed to be 1.247 kg/m^3, which corresponds to a mean temperature of 10° C at sea level.

3. Smoothing of the maps with a 5x5 median filter to remove extreme values caused by the edges of individual satellite images. These effects were

1 The 'energy density' in S-WAsP and in the output .cdf file is given as the mean value of the third power of the wind speed, $\overline{u^3}$ (m^3/s^3).

mostly seen where the coverage was low and the fit of a Weibull function failed.

4. Visualization of the mean wind speed and energy density as gridded maps and contour plots.

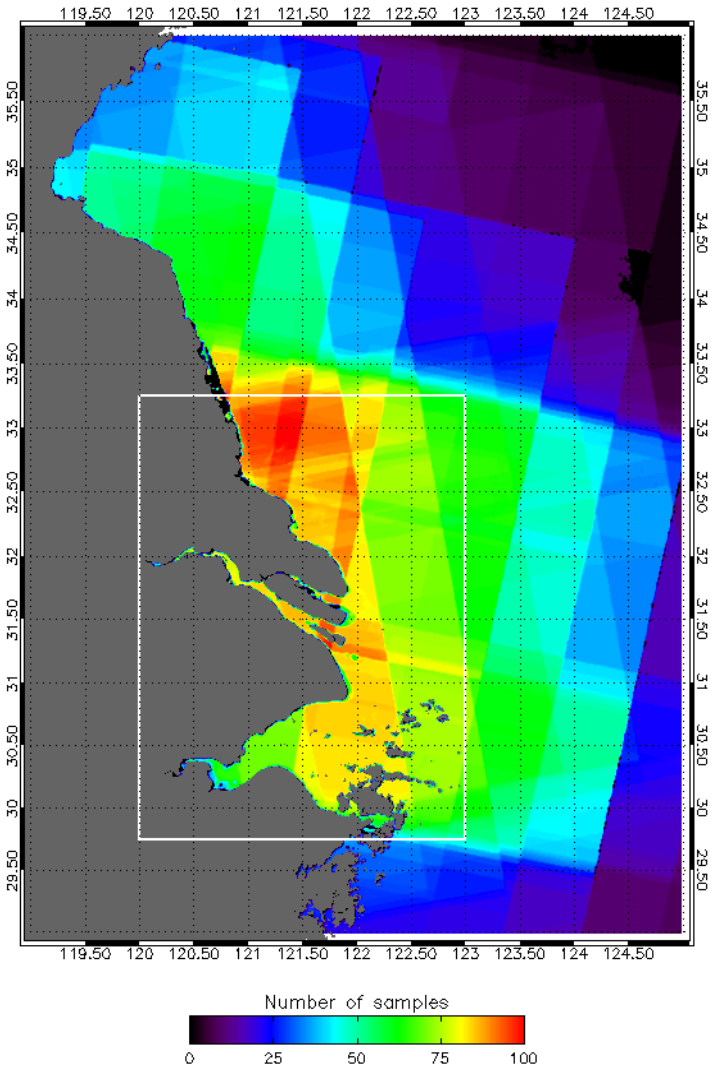

Figure 5. Map showing the number of overlapping satellite scenes for the investigated domain. A smaller domain, with 70 or more satellite samples, was defined for post-processing. This domain is bounded by the white rectangle.

Figure 6 shows a map of the mean wind speed after post-processing. Generally, the mean wind speed at 10 m varies around 7 m/s in the proximity of the coastline and increases up to 9.5 m/s over a distance of 100 km offshore. A reduction of the mean wind speed is seen around the islands in the Hangzhou Bay in the south-eastern part of the domain.

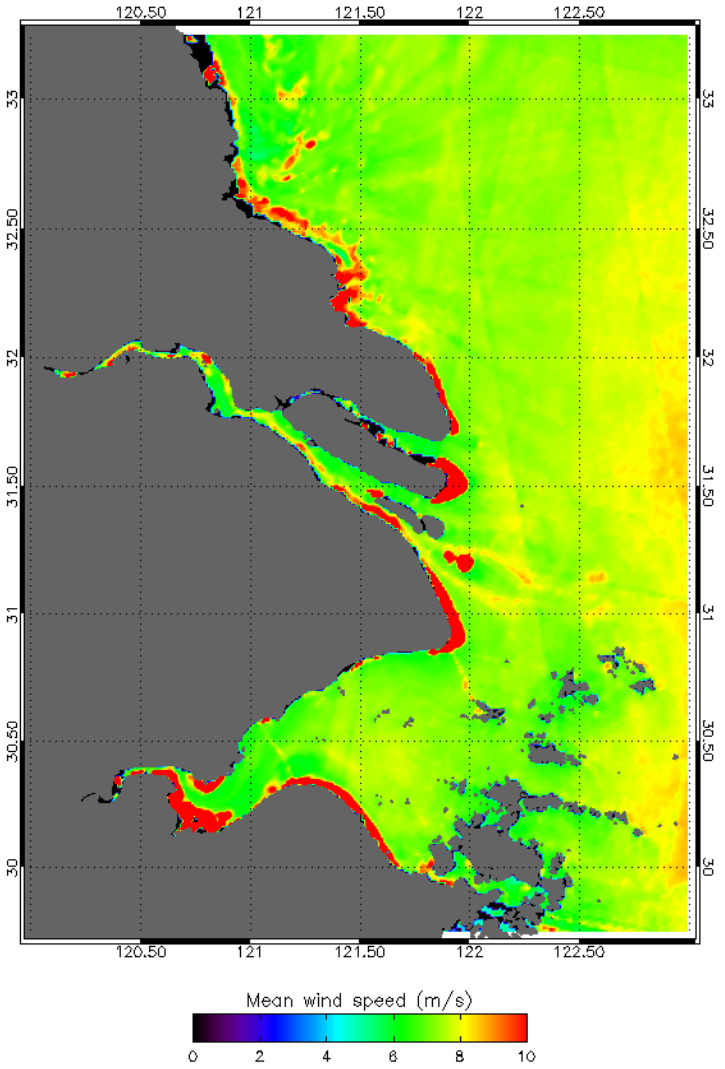

Figure 6. Map of the mean wind speed at 10 m. Very high values (bright red) are caused by exposed sand or mud flats near the cost and are not associated with the wind.

Very high values (bright red) near the cost are caused by exposed sand or mud flats and are not associated with the wind. The exposed sand or mud flats are not included in the land mask that was applied in this analysis. It is possible that other data sets collected within the main project (e.g. bathymetric maps) can be used for a better discrimination between land and sea.

The map of energy densities in Figure 7 emphasizes the variability of the wind resource over the domain. Generally, the energy density increases from 300 W/m^2 near the coast up to 1000 W/m^2 at a distance of 100 km offshore. A significant reduction of the energy density is observed around the islands in the Hangzhou Bay, particularly on the south side of each island. The satellite

data set shows that prevailing winds are from the north in this part of the domain (see section 4.1); therefore sheltering effects are strong on the south side of islands.

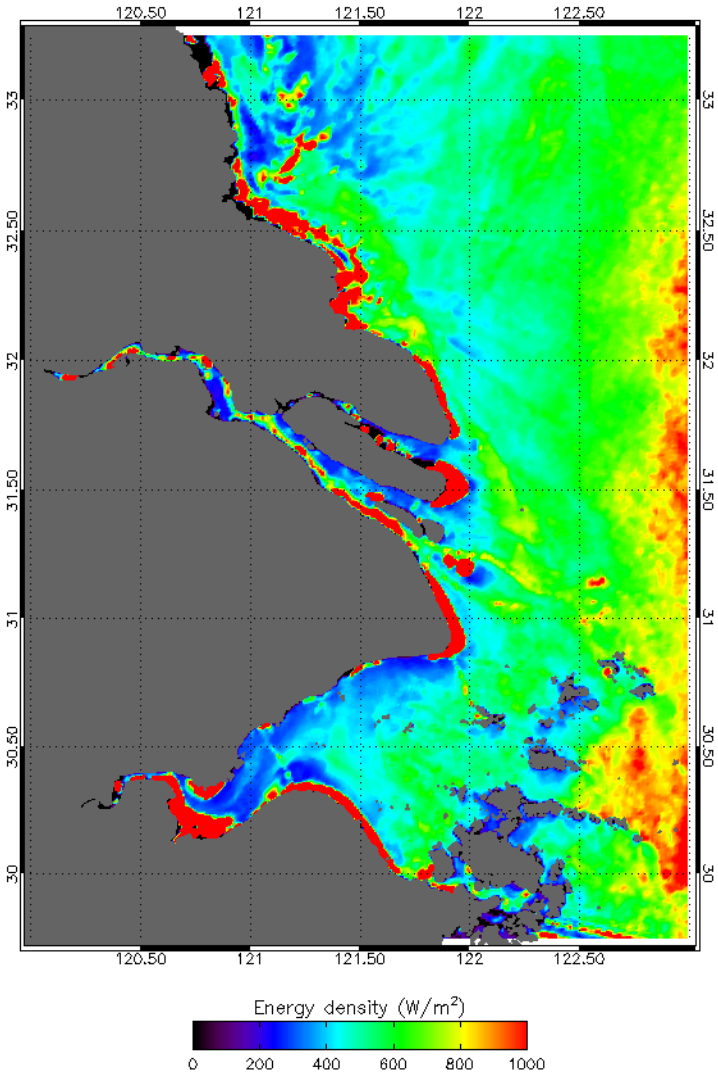

Figure 7. Map showing the energy density at 10 m. Very high values (bright red) are caused by exposed sand or mud flats near the cost and are not associated with the wind.

Sheltering effects of the land are also seen inside the Hangzhou Bay and the Yangtze River Delta. Further north in the domain (around 121E, 32.5N) the energy density is very variable. This variability is associated with bathymetric effects caused by mobile sand bars located within the first 50 km offshore. As anticipated early in the project, the reliability of the satellite SAR image analysis is limited for this section of coastline.

4.2 Site statistics

Site statistics were extracted for two locations that correspond to model grid points used by CMA. The two points are located at coordinates 122.5E, 30N and 122.5E, 32.5N. The positions are shown in Figure 8.

Figure 8. Map showing the location of two points for which S-WAsP site statistics were extracted. The points correspond to grid points in CMA's model. Image courtesy Google Earth.

The site statistics extracted at 122.5E, 32.5N are based on 93 satellite scenes. The distance to the coastline is approximately 100 km. Effects of bathymetry on the SAR imagery were not observed this far offshore. The 93 samples show a mean wind speed of 7.35 m/s (±0.45 m/s) at 10 m. Winds from the north-west are most frequent (20.4%) followed by winds from the south-east (10.8%). Figure 9 summarizes the site statistics and shows a cumulative Weibull fit and a wind rose. Red dots represent the satellite wind observations.

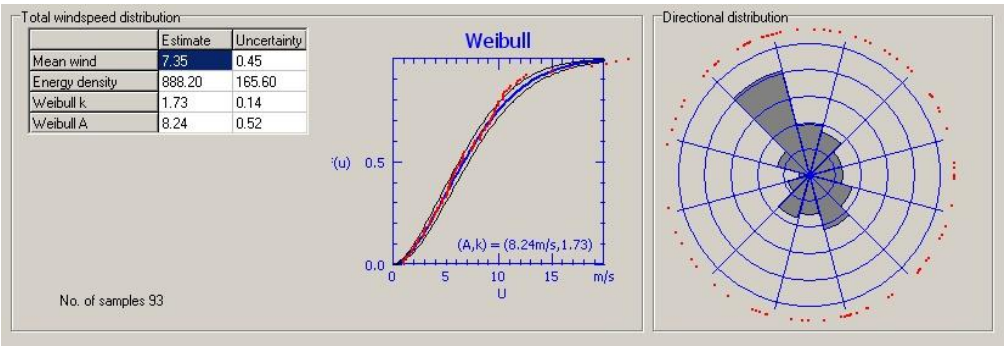

Figure 9. Site statistics for point 122.5E, 32.5N.

Site statistics extracted at 122.5E, 30N are summarized in Figure 10. At this site, 81 overlapping satellite scenes were available. As a consequence of the lower number of samples compared to the site at 122.5E, 32.5N the statistical uncertainty is larger. This site is located less than 10 km east of a group of islands and there is a long chain of islands 25 km to the north of the site. Despite the close proximity to the land, there is no evidence of bathymetry effects in the SAR imagery.

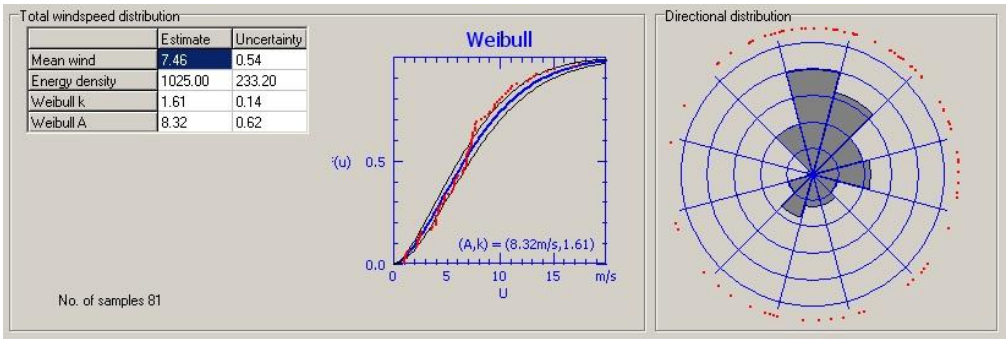

Figure 10. Site statistics for point 122.5E, 30N.

Winds are most frequently from the north (19.8%) and north-east (16%) and the mean wind speed is 7.46 m/s (±0,54) at 10 m. Considering the possibility of wind shadowing caused by the islands to the north, one might have expected a lower mean wind speed at this site compared to the site at 122.5E, 32.5N. A closer investigation of the flow characteristics at this location may reveal mesoscale effects leading to an enhanced wind speed due to topography.

5 Conclusion

The satellite based wind resource mapping project was carried out as scheduled and results of the statistical analysis for the area of interest in China were been delivered on time. The number of ENVISAT images available over the area of interest was restricted to 147, which was less than first anticipated. A precise overview of the spatial distribution of SAR images can only be obtained once the images are ordered and processed.

There are several possibilities of increasing the number of satellite SAR samples, although this would require time and funding beyond the present project. Firstly, the collection of data from the ENVISAT systematic mission will continue as long as there is an interest among the project partners. Secondly, it is possible to submit specific programming requests to ESA in order to ensure coverage over a given site of interest. This requires

submission of a new Category 1 proposal and payment of a programming fee. Finally, the Canadian Space Agency operates two SAR sensors on board the RADARSAT 1 and 2 satellites. ENVISAT and RADARSAT data are equally suitable for ocean wind mapping. However, access to RADARSAT data is normally costly for organizations outside Canada or the US.

Wind resource mapping was performed for the entire area of interest regardless of the number of available satellite samples. The maps were delivered as one multi-layer data file. For the production of colour figures for presentation, results were extracted for a smaller domain, where there were always 70 or more overlapping satellite scenes. This domain covered the southern part of Jiangsu and Shanghai. Here the wind resource statistics were considered relatively robust even though the number of samples was lower than the desired 100 images.

Maps of the mean wind speed and energy density show increasing resources with distance offshore and significant shadowing effects of islands and of the main land. The wind resource maps show realistic values over the Hangzhou Bay where the wind resource is increasing towards the central part of the basin. Wind retrievals over the narrower Yangtze River Delta are more uncertain due to the limited fetch. A verification of the wind maps from satellite SAR against other types of data collected as part of the main project will be interesting. Altogether, the different data sets with their advantages and limitations provide an excellent basis for offshore wind resource assessment in China.

References

Barthelmie, R. J., & Pryor, S. C. (2003). Can satellite sampling of offshore wind speeds realistically represent wind speed distributions. *Journal of Applied Meteorology, 42*, 83-94.

Christiansen, M., Hasager, C., Thompson, D., & Monaldo, F. (2008). Ocean winds from synthetic aperture radar. In R. Nichlos (Ed.), *Ocean Remote Sensing: Recent Techniques and Applications* (pp. 31-54). Kerala, India: Research Signpost.

Christiansen, M. B., Koch, W., Horstmann, J., Hasager, C. B., & Nielsen, M. (2006). Wind resource assessment from C-band SAR. *Remote Sensing of Environment, 105*, 68-81.

Hasager, C. B., Barthelmie, R. J., Christiansen, M. B., Nielsen, M., & Pryor, S. C. (2006). Quantifying offshore wind resources from satellite wind maps: study area the North Sea. *Wind Energy, 9*, 63-74.

Hasager, C. B., Nielsen, M., Astrup, P., Barthelmie, R. J., Dellwik, E., Jensen, N. O., Jørgensen, B. H., Pryor, S. C., Rathmann, O., & Furevik, B. (2005). Offshore wind resource estimation from satellite SAR wind field maps. *Wind Energy, 8*, 403-419.

Hasager, C. B., Peña, A., Christiansen, M. B., Astrup, P., Nielsen, M., Monaldo, F., Thompson, D., & Nielsen, P. (2008). Remote sensing observation used in offshore wind energy. *IEEE Journal of Selected Topics in Applied Earth Observations and Remote Sensing, 1*, 67-79.

Hersbach, H., Stoffelen, A., & de Haan, S. (2007). An improved C-band scatterometer ocean geophysical model function: CMOD5. *Journal of Geophysical Research-Oceans, 112*.

Monaldo, F., Thompson, D. R., Winstead, N. S., Pichel, W. G., Clemente-Colon, P., & Christiansen, M. B. (2005). Ocean wind field mapping from synthetic aperture radar and its application to research and applied problems. *The Johns Hopkins APL Technical Digest, 26*, 102-113.

Monaldo, F. M., & Beal, R. (2004). Wind speed and direction. In C.R.Jackson, & J.R.Apel (Eds.), *Synthetic Aperture Radar Marine User's Manual* (pp. 305-320). Washingon, DC: U.S. Department of Commerce, National Oceanic and Atmospheric Administration.

Nielsen, M., Astrup, P., Hasager, C. B., Barthelmie, R. J., & Pryor, S. C. (2004). *Satellite information for wind energy applications* (pp. 1-57). Roskilde, Denmark: Risø National Laboratory. Risø-R-1479(EN).

Pryor, S. C., Barthelmie, R. J., Mann, J., & Nielsen, M. (2003). Quantifying errors associated with satellite sampling of offshore wind speeds.

Risø DTU is the National Laboratory for Sustainable Energy. Our research focuses on development of energy technologies and systems with minimal effect on climate, and contributes to innovation, education and policy. Risø has large experimental facilities and interdisciplinary research environments, and includes the national centre for nuclear technologies.

Risø DTU
National Laboratory for Sustainable Energy
Technical University of Denmark

Frederiksborgvej 399
PO Box 49
DK-4000 Roskilde
Denmark
Phone +45 4677 4677
Fax +45 4677 5688

www.risoe.dtu.dk